Development and tests of sliding contact line-powered track transporter

Yihua Jiang[1,2], Fang Yang[1,2], Zihao Zhang[1,2], Shanjun Li[1,2,3,4,5*]

(1. *College of Engineering, Huazhong Agricultural University, Wuhan 430070, China*;
2. *China Agriculture (Citrus) Research System, Wuhan 430070, China*;
3. *National R&D Center for Citrus Preservation, Wuhan 430070, China*;
4. *Citrus Mechanization Research Base, Ministry of Agriculture and Rural Affairs, Wuhan 430070, China*;
5. *Key Laboratory of Agricultural Equipment in Mid-lower Yangtze River, Ministry of Agriculture and Rural Affairs, Wuhan 430070, China*)

Abstract: In order to solve the problems of complexity of control systems and the limited power supply of traditional fuel-powered and battery-driven transporters operating in mountainous orchards, a sliding contact line-powered track transporter was designed and manufactured based on theoretical calculations. Key components of the transporter were developed such as a PLC-based (programmable logic controller) control system, a sliding contact power supply, and transmission system, and a position limit device. The functions and performance of designed transporter were tested. The test results showed that the transporter exhibited a high stability of operation with an average operation velocity of 0.70 m/s, the maximum working slope of 48°, the maximum load of 400 kg, and the maximum remote control distance reaching 1482 m. When the power supply circuit of sliding contact line was 108.8 m in length, the maximum voltage drop was 2.4 V, and the maximum power loss was 174.72 W, which were close to the theoretical calculation values. With a single power supply cabinet, the transporter can operate normally for a maximum track distance of 175.69 m. All the technical indicators of the transporter met the design requirements, and the above-mentioned problems such as complexity of the control system and limited energy supply of the traditional mountain orchard transporter were well solved. This study can provide reference for the design and optimization of mountain orchard transporter.

Keywords: mountain orchard, transporter, remote control, sliding contact line, voltage drop
DOI: 10.25165/j.ijabe.20231604.7841

Citation: Jiang Y H, Yang F, Zhang Z H, Li S J. Development and tests of sliding contact line-powered track transporter. Int J Agric & Biol Eng, 2023; 16(4): 68–75.

1 Introduction

The hilly mountainous areas in China account for 2/3 of the country land area with more than 50% of the country's population. However, there are not basically mature mechanical technology and applicable machinery equipment in hilly mountainous areas in China[1-5]. It is difficult to build a road for machinery transportation in the mountainous orchards with large slope (≥25°) terrain. The national citrus industry technology system machinery research team proposed the schemes for developing track conveyor, planning orchard track route, employing track conveyor loading technology, and carrying small-sized mountainous orchard operation management equipment to form entire-process labour-saving operation pattern with track transporter as a carrier carrying small, light and simplified equipment for weeding, digging, spraying, trimming, and others.

In recent years, various types of transporters have been developed in China, and the development of self-propelled monorail fuel-powered transporters[6-8], traction monorail electric transporters[9-12], battery-driven monorail transporters[13,14], and other orchard transport machinery has provided an effective solution to the orchard transportation problem in hilly mountainous areas. Li et al.[15] developed a self-propelled monorail gasoline transporter, optimized its size and structure, and designed a clutch brake linkage device to simplify operation, and their transporter can operate on a 40° slope track with a minimum turning radius of 4 m and a maximum load of 500 kg. Tang et al.[16] developed a traction monorail electric transporter, which achieved steel wire cyclic bidirectional drive and avoided side overturning of monorail transportation, and this transporter could load 300 kg uphill or 500 kg downhill with a maximum working slope of 45° and a minimum turning radius of 4 m. Liu et al.[17] developed a battery-powered transporter with 48V battery powering the motor, and STM32 as the main control module to control the running state of the transporter, and their transporter employed the worm gear structure to realize the self-locking velocity control of the transporter. Self-propelled monorail fuel-powered transporter has such advantages as simple structure, easy operation, high transport efficiency over other transporters, and thus it has been widely applied, but it also has its own disadvantages such as serious exhaust pollution, operation noise, and remote control application difficulty. Traction monorail electric transporter exhibits the advantages such as simple maintenance, remote control convenience, but the use of steel wire limits traction distance. Battery-driven monorail transporters have the advantage of control convenience, but limited, energy supply and low charging efficiency pose obvious disadvantages.

In this study, a sliding contact line-powered transporter was designed so as to solve the problems of electric control complexity of self-propelled monorail fuel transporters and to break through the

Received date: 2022-08-05 **Accepted date:** 2023-07-18
Biographies: Yihua Jiang, PhD candidate, research interest: intelligent equipment for fruit production and multi-robot coordinated control, Email: yihuajiang.hzau@foxmail.com; **Fang Yang**, Associate Professor, research interest: networked control system and multi-robot coordinated control, Email: yangfang@mail.hzau.edu.cn; **Zihao Zhang**, MS, research interest: intelligent equipment for fruit production. Email:1954114076@qq.com.
***Corresponding author: Shanjun Li**, Professor, research interest: intelligent equipment for fruit production. College of Engineering, Huazhong Agricultural University, Wuhan 430070, China. Tel: +86-13071289256, Email: shanjunlee@mail.hzau.edu.cn.

energy supply limitation of battery-driven monorail transporters. Our designed transporter adopts brushless direct current (DC) motor as the power source with its power supply device built on the ground. The electric power required by the motor and the control box is supplied by the sliding contact line installed along the track and the collector moving with the transporter. The remote control module and programmable logic controller (PLC) control program were used for start/stop, velocity regulation, and state switching of the transporter, achieving efficient control of the machine. According to the mountain working requirements, our transporter has a dead weight of 150 kg, a maximum load of 400 kg and a maximum working slope of 48°. In order to balance the transport efficiency and smoothness of the transporter, the running velocity of the transporter was designed to be 0.7 m/s.

2 Design and principle of the transporter system

2.1 Structure

The overall structure of the transporter system is shown in Figure 1. The sliding contact transporter system includes ground power supply device, mobile equipment power supply device, conveying device, and control system. The power supply system of the transporter consists of ground power supply device and mobile equipment power supply device to ensure the power supply and transmission. The conveying device includes belt conveyor and worm gearbox conveyor. The control system is integrated in the electronic control box to take the control over the transporter, including start/stop, velocity regulation, forward and reverse.

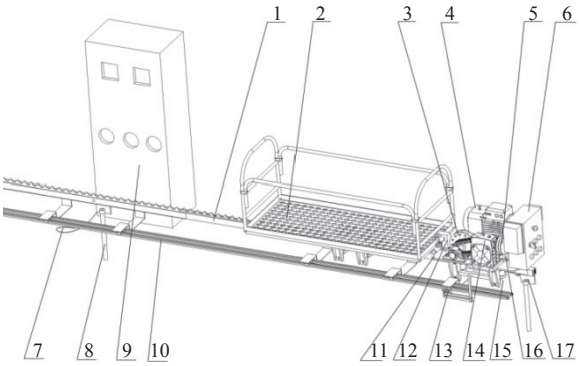

1.Track 2.Trailer 3.Drive wheel 4.Worm gear reducer 5.Belt 6.Electric control box 7.Transmission wire 8.Standing pile 9.Power supply cabinet 10.Sliding contact line 11.Chassis 12.Universal joint 13.Collector 14.Worm gear reducer 15.T-shaped wheel 16.Driven wheel 17.Pipe fasteners

Figure 1 Schematic of transport system structure

2.2 Working principle

When the transporter is powered on, the power supply cabinet outputs 48V DC to the two sliding contact lines after the 220 V alternative current (AC) power was transformed and rectified into 48V DC. The two collectors extended from transporter motor contact the two sliding contact lines so that the sliding contact lines, the collector, and the motor form a complete circuit. The power generated by the motor is transmitted to the worm gear reducer through the pulley, and then the power is transmitted to the drive wheel through the output shaft of the worm gear reducer. Subsequently, the drive wheel engages with the main rail gear rack to make the transporter function. The main parameters of the sliding contact line-powered transporter are listed in Table 1.

3 Design of transporter hardware system

3.1 Power unit design

The transporter is mainly affected by gravity, the support force of the slope, and the friction force from the track. When the transporter is running at full load and uniform velocity, the traction force of the transporter itself needs to be balanced with the external forces. The force analysis of the transporter is shown in Figure 2.

Table 1 Main parameters of transporter

Parameters	Values
Shape size/mm	2600×620×800
Rated power/kW	5.0
Machine weight/kg	150
Operation velocity/m·s^{-1}	0.2-0.7
Maximum load capacity/kg	≤400
Maximum slope angle/(°)	≤48
Minimum turning radius/m	4

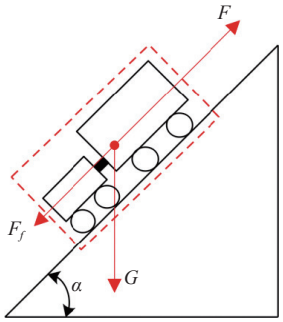

Note: G is the gravity acting on the transporter and the cargo box, N; F_f is the frictional force acting on the transporter and the cargo box, N; F is the traction force generated by the transporter, N; α is the maximum slope of the mountain track, (°).

Figure 2 Forces acting on transporter

The force acting on the transporter and power generated by the transporter are calculated according to the following equations:

$$F = G\sin\alpha + F_f = (m_1 + m_2)g\sin\alpha + \mu(m_1 + m_2)g\cos\alpha \quad (1)$$

$$P_1 = \frac{F \times v_1}{\eta_0 \times \eta_1} \quad (2)$$

where, m_1 is the mass of the transporter, kg; m_2 is the mass of the load, kg; g is the acceleration of gravity, m/s^2; μ is the combined coefficient of friction between the drive wheel and the main track rack and friction between the T-shaped wheel and the side of the main track; v_1 is the velocity of the transporter, m/s; η_0 is the efficiency of the belt conveying; η_1 is the efficiency of the worm gear conveying.

The maximum velocity v_1 is set as 0.7 m/s; the maximum load$m_2$is set as 400 kg; the maximum gradient α is set as 48°; and the mass of the transporter is 150 kg. The values of g, μ, η_0, η_1 are set as 9.8 m/s^2, 0.14, 0.94, and 0.7 in this study. According to Equation (2), P_1 is calculated as 4.79 kW.

According to the power required by the transporter, a brushless DC motor with a high loading current and a long service life is selected with its relevant parameters as listed in Table 2.

3.2 Transmission design

In order to simplify the conveyor structure and to increase the

Table 2 Brushless DC motor parameters

Parameters	Values
Rated voltage/V	48
Rated power/kW	5.0
Rated rotating velocity/r·min^{-1}	1500
Overload current/A	106

operation efficiency, two types of conveying devices were adopted: worm gear conveyor and belt conveyor. The worm gear reducer has a compact structure, enabling smooth transportation. Through the transmission method of the worm gear reducer, high-torque output is generated, thereby increasing the payload capacity of the transporter. Moreover, its design allows for self-locking of the transporter on slopes, preventing accidental sliding. The belt conveyor connects the electric motor output shaft to the input shaft of the worm gear reducer in a flexible manner, cushioning the impact on rigid connections when the motor stops abruptly. This makes the transporter operation smoother and also reduces potential damage to the loaded goods in the cargo box. The installation of the reducer is depicted in Figure 3.

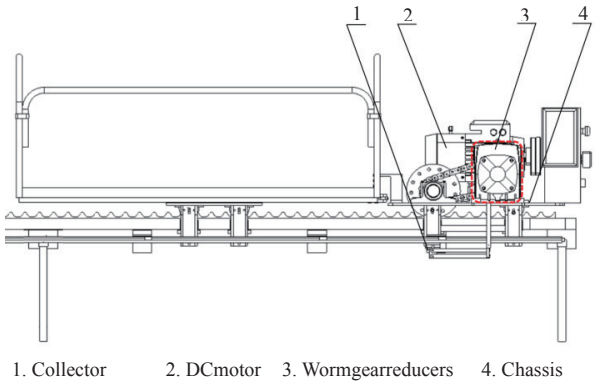

1. Collector 2. DC motor 3. Worm gear reducers 4. Chassis

Figure 3 Schematic of reduction gearbox installation

The drive wheel and the worm gear are installed onto the same shaft, the belt conveying ratio and the worm gear conveying ratio are i_1 and i_2, respectively. The total conveying ratio (i) is calculated according to the following equations:

$$n_2 = \frac{n_0}{i_1 \times i_2} \tag{3}$$

$$V_1 = \frac{\pi \times D_1 \times n_2}{60} \tag{4}$$

$$i = i_1 \times i_2 \tag{5}$$

where, n_2 is the drive wheel rotating velocity, r/min; n_0 is the DC brushless motor rotating velocity, r/min; D_1 is the drive wheel diameter, m; i_1 is the belt conveying ratio; i_2 is the worm gear conveying ratio; and i is the total conveying ratio.

The DC brushless motor rotating velocity$n_0$is 1500 r/min; the drive wheel diameter D_1 is 0.195 m; the transporter velocity V_1 is set as 0.7 m/s. Drive wheel rotating velocity n_2 is calculated as 68.6 r/min. Total conveying ratio i is calculated as 22.

The total conveying ratio is assigned to all levels of conveying ratio. The larger the worm gear conveying ratio, the better the braking effect of the transporter when it goes downhill, whereas the smaller the belt conveying ratio, the larger the small pulley wrap angle, the better the conveying performance. Considering these, the belt conveying ratio i_1 was set as 1.1, and worm gear conveying ratio$i_2$was set as 20.

3.3 Power supply unit design

There are three types of tram power supply systems including overhead contact network power supply, energy storage power supply, and ground sliding contact power supply[18-20]. The overhead contact network is limited to overhead space restrictions, and it needs to be equipped with lightning protection measures. For energy storage power supply, energy storage is time-consuming with low efficiency. When the system efficiency, the installation space, and cost are taken into consideration, the ground sliding contact line power supply was selected and the transporter power supply unit was designed and manufactured[21].

The transporter power supply device has the following functions. Firstly, it can convert 220 V industrial-frequency AC power into 48 V DC power, and this power supply device is connected to the sliding contact line. Secondly, it can real-time monitor the current and voltage state of the transporter, and it is equipped with current overload protection device and a battery backup power supply to prevent accidents caused by industrial frequency AC power failure. According to the power demand, DC power supply device is designed, as shown in Figure 4. The actual power supply unit is shown in Figure 5.

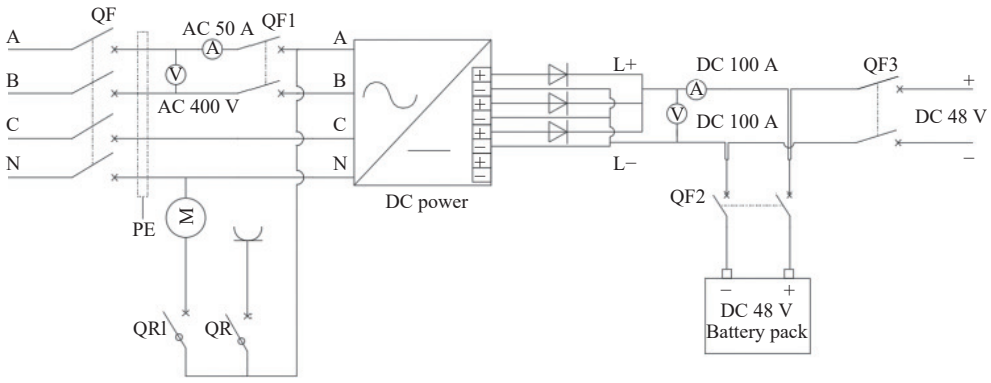

Figure 4 Schematic of DC power supply device design

3.4 Design of power transmission device

The common mobile electricity transmission method for electrified rail transport is the third rail electricity transmission with low installation and maintenance cost[22]. The third rail electricity transmission has three electricity current reception methods, including upper part, side, and lower part current reception. Considering that the working environment of the transporter is mountainous area, it is easy for water, mud, and rocks to accumulate due to the poor climate. For the sake of stable power supply and convenient maintenance, the lower part current reception method is selected so as to elevate sliding contact line to avoid the adverse effects of above-mentioned factors. According to the maximum current of the DC brushless motor, TLHX-200A two-pole sliding contact line was selected with its main parameters as listed in Table 3. The sliding contact line track is fixed to the subtrack completely welded below the main track with sliding

Figure 5 Actual power supply unit

Table 3 Sliding contact line parameters

Parameters	Values
Cross-section area/mm^2	110
Load current /A	200
Resistivity/Ω·km^{-1}	0.301
Reactance/Ω·km^{-1}	0.325
AC voltage/V	≤660
DC voltage/V	≤1000

contact line track parallel to the main track. The collector is fixed by the bracket and connected to the DC brushless motor. The actual installation of tracks is shown in Figure 6.

Figure 6 Track installation method

4 Design of transporter software system

4.1 Overall scheme of control system

PLC is control core of the transporter control system, and the control system functions include remote control over transporter start, stop, and velocity regulation. The control system structure is shown in Figure 7. The control flow of the transporter is shown in Figure 8. The Siemens S7-200 series PLC (CPU224) was selected as control system processor, and the control system I/O (Input/Output) address allocation is shown in Table 4.

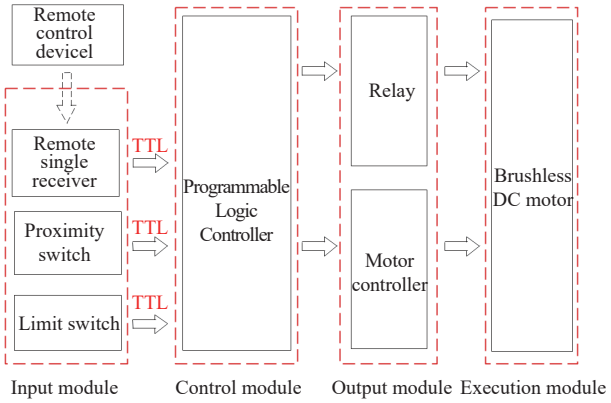

Figure 7 Schematic of control system structure

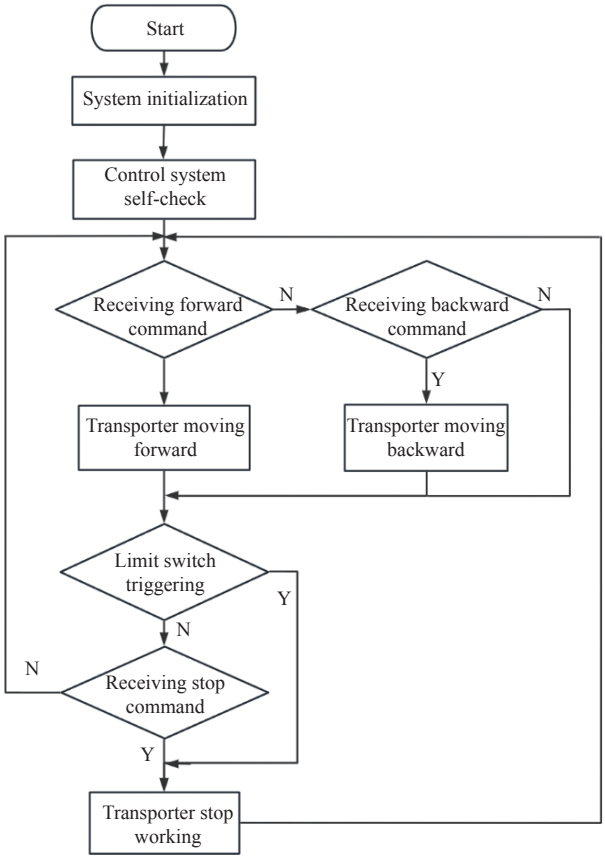

Figure 8 Control flow chart

Table 4 Sliding contact line parameters

Item	I/O address allocation								
Input address	I0.0	I0.1	I0.2	I0.3	I0.4	I1.0	Q0.0	Q0.1	Q0.2
Description of input	Forward command	Backward command	Stop command	Limit switch at the front	Limit switch at the rear	Proximity switch	Motor forward rotation	Motor Reversal rotation	Motor Stop

4.2 Velocity control system

The PID-based (Proportional-Integral-Derivative) automatic velocity control function of transporter allows its operation velocity to maintain within the range of 0.7±0.08 m/s under various loads and slopes[23,24]. An NPN (Negative-Positive-Negative) type proximity switch was installed onto the driven wheel for velocity sampling. The proximity switch installation is shown in Figure 9.

The real-time velocity of the transporter is calculated according to the following formula:

$$V_2 = D_2 \cdot M \cdot f \tag{6}$$

where, V_2 is the real-time velocity of the transporter, mm/s; D_2 is the gear distance (4.6 mm); M is the number of cylindrical rollers of the driven wheel (12); f is the detection frequency of proximity switch, Hz.

The real-time detection frequency obtained from the proximity switch is introduced into Equation (6) to calculate the real-time velocity, which is fed back to the PID controller for velocity regulation.

5 Test of transporter

5.1 Performance test of the transporter

The performance test of the transporter was carried out at the Agricultural Science Institute in Wuhan, Hubei Province. The

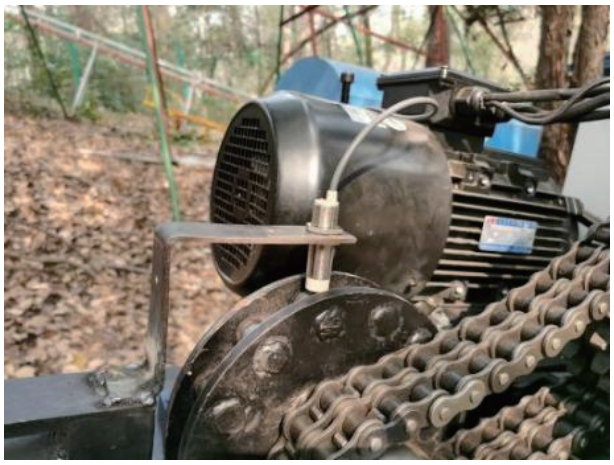

Figure 9 Proximity switch installation

maximum slope of the track at the test site was 48°, as shown in Figure 10. The test equipment comprised sliding contact line-powered track transporter, GNSS receiver, GNSS base station, clamp-on ammeter, voltmeter, electronic scale, rocks, stopwatch, tape measure, etc. Both the M900SE model GNSS receiver and the M300 model GNSS base station are products of ComNav Technology Ltd. The GNSS positioning measurements achieved a vertical and horizontal accuracy of ±8 mm and ±15 mm, respectively. For the tests, rocks served as the load, weighed using an electronic scale, with the transporter handling a load range from 0 to 400 kg.

Figure 10 Test site of transporter (Test Site 1)

The transporter is controlled in two ways, including the box panel control and handheld remote control. The transporter can complete functions such as moving forward and reversal, emergency braking, and automatic limit stop at any point on the track. The transporter has been tested several times under extreme conditions. It can carry a load of 400 kg on a 48° slope, and under this conditions emergency braking and frequent start forward and reverse are tested with a 100% response success rate. The test results indicate that the transporter's design meets the slope angle and load capacity requirements.

5.2 Velocity test in multiple-states

The track, upon measurement with a tape measure, had a total length of 78 m. The segments of the track with slopes of 48° and 28° were approximately 11.5 m and 19.2 m in length, respectively. The operating time of the transporter, under varying conditions, was recorded using a stopwatch, comprising ten individual measurements. Using the formula $v=s/t$, the transporter's speed was determined, and the average speed was calculated as $v_{\_avg}=\Sigma v/n$. Figure 11 depicts the mean speed of the transporter across diverse operational states. The operation speed fluctuated within –10.8% and +6.5% of the set speed of 0.7 m/s, thus demonstrating the transporter's excellent velocity stability.

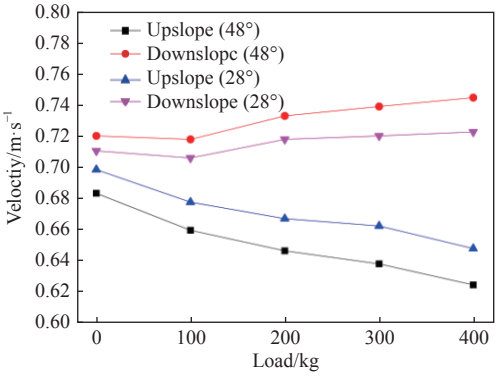

Figure 11 Transporter velocity in multiple states

5.3 Braking test in multiple states

Two types of braking mechanisms are identified for the transporter: active braking, controlled by a remote or button, and passive braking, initiated by a limit switch. Passive braking activated by the limit switch was chosen to mitigate the response time error due to human interaction (Figure 12).

Figure 12 Limit switch contacts baffle

The entire braking process is divided into a delayed phase and an actual braking phase. The delay period refers to a short delay caused by the electromagnetic de-energized brake after the limit switch contact the baffle, and the delay period is followed by the actual braking period. The time length of delay period is random after the limit switch contact the baffle, and thus the braking distance fluctuates on the same slope under the same load conditions. The braking performance of the transporter under various operational conditions is depicted in Figure 13. With the rise in load and slope, the duration of the actual braking cycle (from onset to complete stop) increases. Significantly, an increase in the transporter's load enhances the standard deviation in braking distance, thus complicating the prediction of the actual braking distance. However, even under severe conditions of a maximum load of 400 kg and a slope of 48°, a braking distance of 593 mm fulfills the operational demands of orchard tasks in mountainous terrains.

5.4 Remote control test in multiple states

Remote control tests were conducted at the Shizishan Orchard in Huazhong Agricultural University and the Wuhan Academy of Agricultural Sciences in Hubei Province, China. The transporter was equipped with a TX-904-LFW2 model remote control and

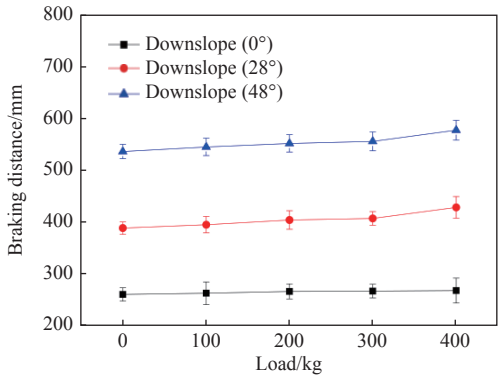

Figure 13 Transporter braking performance in multiple states

receiver, manufactured by Tianjin Boao Electronic Technology Co., Ltd. Upon the transmission of a signal from the remote control, the receiver's response was assessed to validate the successful transmission and receipt of commands. This test was conducted at various locations and repeated 50 times, allowing the calculation of a response success rate, denoted as C, using the formula $C=(c_i/50)\times100\%$. The GNSS receiver was utilized to record the longitude, latitude, and altitude information of the locations where the success rate, C, exceeded 95%. The effective remote control distance was ascertained by calculating the actual straight-line distance between the coordinates of the remote control position (A_x) and the transporter position (A_o). Concurrently, the altitude difference was computed as the discrepancy between the altitude of the remote control position ($H_{\_Ax}$) and the transporter position ($H_{\_Ao}$). The results of the remote control tests are listed in Table 5.

Table 5 Remote control test results

Test location	Test environment	Altitude difference ($H_{\_Ax}$–$H_{\_Ao}$)/m	Reverse slope	Valid remote distance/m
Shizishan Orchard in Huazhong Agricultural University	Wooded environment (1500-1900 trees·hm^{-2})	17.06	No	605
	Wooded environment (1500-1900 trees·hm^{-2})	–16.71	No	579
	Wooded environment (1500-1900 trees·hm^{-2})	–19.59	Yes	317
	Wooded environment (100-300 trees·hm^{-2})	28.34	No	933
Wuhan Academy of Agricultural Sciences	Wooded environment (600-800 trees·hm^{-2})	4.37	No	872
	Open environment	0.26	No	1482

As observed from Table 5, the shortest valid control distance occurred when the remote control position was on a slope opposite to that of the transporter's location. With increasing vegetation density, the valid control distance decreased. The valid control distance was greater when the altitude difference ($H_{\_Ax}$–$H_{\_Ao}$) was positive ($H_{\_Ax}$–$H_{\_Ao}$>0), compared to when it was negative ($H_{\_Ax}$–$H_{\_Ao}$<0). Therefore, the valid distance of remote control is inversely proportional to vegetation density but directly proportional to altitude difference, with a non-reverse slope location providing superior results than a reverse slope. The signal attenuation varies in different environments where the mountain transporter operates, and this result provides a reference for considering the effective remote control distance in operating the transporter.

5.5 Actual power and power loss tests

The power test of transporter was carried out at the Shizishan Orchard of Huazhong Agricultural University, and the track was built with a maximum slope of 30°, as shown in Figure 14.

Figure 14 Test site of transporter (Test site 2)

The electrical power required by the transporter is transmitted through the power supply cabinet, the sliding contact line, and the collector. The real-time current I was measured using a clamp-on ammeter and the real-time voltage U was measured using a voltmeter. The real-time power under different load conditions was calculated according to the formula $P=U\cdot I$ (Figure 15), and the maximum power is shown in Table 6.

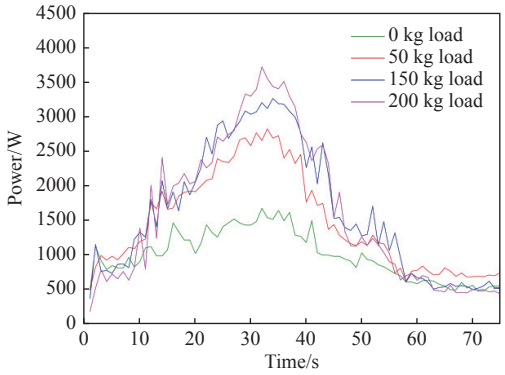

Figure 15 Transporter power at 4 different loads

Table 6 Transporter maximum power in multiple operation conditions

Groups	Maximum power/W			
	0 kg load	50 kg load	150 kg load	200 kg load
30° upslope	1660	2816	3258	3720
20° downslope	615	822	943	715
Flat slope	1451	1908	2249	2580

The peak currents I_{a1} = 33.8 A, I_{a2} = 55.0 A, I_{a3} = 63.9 A and I_{a4} = 72.8 A at the transporter loads of 0 kg, 50 kg, 150 kg, and 200 kg, respectively. The operation states of the transporter at different time points were as follows. Within 0-19 s, the transporter was running on a flat slope at the bottom of the hill; Within 20-43 s, the transporter was running uphill (a 30° slope); Within 44-57 s, the transporter was running on a flat slope at the top of the hill; Within 58-75 s, the transporter was running downhill (a 20° slope). Our data showed that at the 4 load cases (0 kg, 50 kg, 150 kg, and 200 kg), the peak power of transporter occurred during uphill course on a 30° slope. In addition, the power at different loads during the flat slope running course was relatively close. The actual power first increased and then decreased with the increasing load when transporter went downhill. The possible reason might be that when transporter went downhill with high load, the gravity component of

the goods along the track provided a large amount of forces to the transporter. Therefore, the less power from DC motor was required to maintain the normal operation of the transporter.

The circuit of the sliding contact line contains the live wire and the naught wire, and the length of circuit is twice the length of the track. Therefore, the internal resistance of the sliding contact line can be calculated according to the following formula:

$$R_1 = 2L \cdot R_x \tag{7}$$

where, R_1 is the internal resistance of the sliding contact liner, Ω; R_X is the resistivity per unit length of the sliding contact line (0.301 Ω/km); L is the length of the track (54.4 m). According to Equation (7), the internal resistance of sliding contact line R_1 was calculated as 0.032 Ω.

The common working condition was as follows: a load of 200 kg by a single transporter and the maximum current I_{a4} of 72.8 A. The calculation formula of the sliding contact line pressure drop ΔU_1 is as follows:

$$\Delta U_1 = I_{a4} \times R_1 \tag{8}$$

According to Equation (8), $\Delta U_1 =$ 2.33 V. The theoretical maximum power loss P_3 was calculated according to the following formula:

$$P_3 = R_1 \times I_{a4}^2 \tag{9}$$

According to Equation (9), P_3=169.59 W.

Under the same working condition (a load of 200 kg by a single transporter), the actually measured initial end maximum voltage $U_1 =$ 53.0 V, output end minimum voltage $U_2 =$ 50.6 V, and thus the actual voltage drop was calculated as $\Delta U_2 = U_1 - U_2 = 2.4$ V. Based on it, the actual maximum loss of power P_4 is calculated as follows:

$$P_4 = \Delta U_2 \cdot I_{a4} \tag{10}$$

According to Equation (10), P_4=174.72 W.

The calculation results showed that the theoretical loss power P_3 was 97.06% of the actual loss power P_4, and the closeness between P3 and P4 indicated the accuracy of our power calculation. Thus, our results provide a reference for subsequent selection and optimization of sliding contact lines.

5.6 Voltage drop test

According to the national standard GB/T 755-2019, the motor operation conditions are met when operation voltage is ±10% of the rated voltage. The rated voltage of the motor was selected as 48 V, and the corresponding operating voltage range was 43.2-52.8 V. According to the theoretical voltage range value, an adjustable silicon chain electric control box was developed and installed between the power supply cabinet and the sliding contact line. The voltage range was adjustable between 42.6 V and 53.1 V, with 0.7 V per gear and 15 gears in total.

The voltage of the silicon chain electric control box was adjusted to the voltage range of 45.4-53.1 V to ensure the normal operation of the transporter with a load of 200 kg. When a single power supply cabinet supplies power for the normal operation of a single transporter, the longest circuit is calculated according to the following equation:

$$S = \frac{\Delta U_3}{I_{a4} \cdot \mathrm{R_x}} \tag{11}$$

where, S is the longest circuit under normal operation of a transporter, m; ΔU_1 is the actual normal operation voltage difference between the maximum and the minimum (7.7 V); I_{a4} is the actual normal operation maximum current (72.8 A); R_x is the resistivity of the sliding contact line per unit length (0.301 Ω/km). According to Equation (11), S =351.39 m. Since the length of the sliding contact line circuit is twice the length of the track, the maximum track distance for the normal operation of a single transporter powered by a single power supply cabinet was 175.69 m. Therefore, based on these test results, it is known that when there is a need to lay long-distance tracks in mountain orchards, more power supply cabinets in parallel need to be evenly installed within the track system.

6 Conclusions

This study designed and developed a sliding contact line-powered transporter specifically tailored for mountain orchards. Based on performance tests, velocity tests, braking and remote control tests in multiple states, power tests, voltage drop tests, and other tests, the main conclusions were as follows.

(1) The designed transporter can perform multiple tasks in a mountainous environment and implement such functions as forward, reverse, braking, limit braking, and PID velocity regulation. As a result, the problem of limited energy supply by traditional electric motor-driven transporter is well solved. This study lays a solid foundation for the subsequent research on multiple transporters' collaborative work.

(2) Test results indicate that the transporter's operating speed consistently fluctuates within –10.8% and +6.5% of the set speed of 0.7 m/s. The maximum operational slope of the transporter was determined to be 48°. Its load capacity maxed out at 400 kg. The braking distance extended to a maximum of 593 mm, while the remote control distance reached up to 1482m. These results satisfy the design requirements for mountain transport operations.

(3) The results also show that when power supply circuit is 108.8 m, the maximum voltage drop at the output end is 2.4 V. The theoretical power loss of sliding contact line is 169.59 W, which is 97.06% of the actual power loss (174.72 W). Finally, the longest track distance is 175.69 m in the case of normal operation of a single transporter powered by a single power supply cabinet.

Acknowledgements

The authors acknowledge that this work was supported by the Special Funds for the Construction of Industrial Technology System of Modern Agriculture (Citrus) (Grant No. CARS-26), National Key R&D Program (Grant No. 2020YFD1000101), Hubei Province Key R&D Program (Grant No. 2021BBA091).

[References]

[1] Zheng Y J, Jiang S J, Chen B T, Wu H T, Wan C, Kang F. Review on technology and equipment of mechanization in hilly orchard. Transactions of the CSAM, 2020; 51(11): 1–20. (in Chinese)

[2] Luo X W, Liao J, Hu L, Zang Y, Zhou Z Y. Improving agricultural mechanization level to promote agricultural sustainable development. Transactions of the CSAE, 2016; 32(1): 1–11. (in Chinese)

[3] Zhao Y, Xiao H R, Mei S, Song Z Y, Ding W Q, Jin Y, et al. Current status and development strategies of orchard mechanization production in China. Journal of China Agricultural University, 2017; 22(6): 116–127. (in Chinese)

[4] Liu P Y, Wang C Y, Li H T, Zhang M M, Wei W J, Zhang S Y. Terrain adaptive and dynamic leveling agricultural chassis for hilly area. Transactions of the CSAM, 2018; 49(2): 74–81. (in Chinese)

[5] Liu D W, Xie F P, Li X, Wang X L. Design and experiment of small lifting platform in orchard. Transactions of the CSAE, 2015; 31(3): 113–121. (in Chinese)

[6] Li S J, Xing J J, Zhang Y L, Meng L, Fan Q Z. 7YGS-45 Type Self-

propelled Dual-track Mountain Orchard Transport. Transactions of the CSAM, 2011; 42(8): 85–88. (in Chinese)

[7] Zhang J F, Zhang Y L, Zhang T J, Li S J, Meng L. Design of the remote control system for self-propelled mountainous monorail transporter. Journal of Huazhong Agricultural University, 2012; 31(6): 792–796. (in Chinese)

[8] Zhang J F, Li J Y, Zhang Y L, Li S J, Meng L. Design of remote control monorail transporter for mountainous orchard. Transactions of the CSAM, 2012; 43(2): 90–95. (in Chinese)

[9] Meng L, Zhang Y L, Zhang W Y, Liu J, Li S J, Li M Z. Design of trailed trackless mountain orchard transporter with remote control. Journal of Huazhong Agricultural University, 2015; 34(4): 125–129. (in Chinese)

[10] Li J X, Zhong M Y, Zhang Y L, Bao X L, Li S J, Liu M D, et al. Optimized design of the power consumption test of mountain orchard transporters. Int J Agric & Biol Eng, 2021; 14(5): 107–114.

[11] Xie D B, Chen L, Liu L C, Chen L Q, Wang H. Actuators and sensors for application in agricultural robots: A review. Machines, 2022; 10(10): 913.

[12] Li J X, Li S J, Zhang Y L, Liu M D, Gao Z Y. Development and test of hydraulic driven remote transporter. Int J Agric & Biol Eng, 2021; 14(2): 72–80.

[13] Li Z, Hong T S, Sun T B, Ouyang Y P, Luo Y Q. Design of battery powered monorail transporter for mountainous orchard. Journal of Northwest A&F University (Natural Science Edition), 2016; 44(6): 221–227. (in Chinese)

[14] Luo Y Q, Hong T S, Li Z, Zeng J Y, Sun T B, Li J N. Development of control device for an electric drive monorail vehicle in mountain orchard. Journal of Northwest A&F University (Natural Science Edition), 2016; 44(3): 227–234. (in Chinese)

[15] Li X J, Zhang Y L, Zhang W Y, Ling X P. Design and improvement of the remote control self-propelled monorail transporter for mountainous orchard. Journal of Huazhong Agricultural University, 2014; 33(5): 117–122. (in Chinese)

[16] Tang X L, Zhang Y L, Li X J. 7YGD-45 type electrically operated remote-controlled single-track orchard transport. Hubei Agricultural Sciences, 2013; 52(2): 443–447. (in Chinese)

[17] Liu Y, Li Z, Hong T S, Lyu S L, Song S R, Huang S P. Design of drive system for battey-drive monorail transporter for mountainous orchard. Transactions of the CSAE, 2017; 33(19): 34–40. (in Chinese)

[18] Li Q, Shang W L, Yan Y, Chen W R. Research on braking distribution and braking energy recovery for novel power supply model tram. Proceedings of the Chinese Society of Electrical Engineering, 2020; 40(7): 2285–2294. (in Chinese)

[19] Dai C H, Fu X T, Du Y, Guo A, Chen W R. Supercapacitor thermal behavior of trams with different spatial structures. Journal of Southwest Jiaotong University, 2020; 55(5): 920–927. (in Chinese)

[20] Wang Y, Yang Z P, Lin F, Li F, An X K. Dynamic ratio distribution strategy for hybrid storage system of tram. Transactions of China Electrotechnical Society, 2019; 34(A01): 405–413. (in Chinese)

[21] Zhao H J, Chen W J, Shen H B, Bian K. Research on the lightning protection effect of metro overhead ground wire. Journal of Railway Engineering Society, 2015; 32(1): 122–128. (in Chinese)

[22] He Y Y, Huang K, Wang T, Zhang G X. Overview of traction power supply system for rail transportation. Journal of Railway Science and Engineering, 2016; 13(2): 352–361. (in Chinese)

[23] Zhu R T, Wu H T. Design of DC motor velocity regulation system based on incremental PID algorithm. Instrument Technique and Sensor, 2017; 7: 121–126. (in Chinese)

[24] Jing J L, Wang Y C, Zhu Y Q. Fuzzy parameter adaptive PID control of brushless DC motors. Control Engineering of China, 2018; 25(5): 915–919. (in Chinese)